PUBLICATION IV

On the role of particle state and deposition procedure on mechanical, tribological and dielectric response of high velocity oxy-fuel sprayed alumina coatings

In: Materials Science and Engineering 2005.
Accepted for publication.

On the role of particle state and deposition procedure on mechanical, tribological and dielectric response of high velocity oxy-fuel sprayed alumina coatings

E. Turunen, T. Varis, S.-P. Hannula*[1]
VTT Industrial Systems, Espoo, Finland

A. Vaidya, A. Kulkarni, J. Gutleber, S. Sampath, H. Herman,
State University of New York, Stony Brook, NY, USA

* Corresponding author: Tel: +358-20-722 5425, Fax: +358-20-722 7069
Email: erja.turunen@vtt.fi
Address: VTT, P.O.Box 1703, FI-02044 VTT, Finland

[1] S-P. Hannula is a joint professor of Helsinki University of Technology and VTT Industrial Systems

Key words: *Thermal spray, HVOF, process optimization, diagnostic, alumina, mechanical properties, thermal and electrical properties*

Abstract

It is well known that the high velocity oxy-fuel based thermal spray process impart high density and reduced porosity in coatings compared to those produced by other ambient thermal spray processes. The benefits of HVOF have largely remained in the domain of metals and cermets and limited investigations have been carried out in ceramic coatings. The ability to produce high density ceramic coatings (e.g. alumina) offers potential in high performance applications in the field of wear, corrosion resistance, and dielectric coatings. However, due to extreme operational limits of the HVOF process, the fundamentals of process-structure-property relationships are not fully understood.

In this paper, we report an integrated approach to establish processing-microstructure-property correlations in order to optimize coatings for such

applications. This approach involves diagnostic studies, microstructure development and its resultant influence on properties of high velocity oxy-fuel (HVOF) sprayed alumina coatings. The diagnostic studies were aimed to investigate the effects of fuel gas/oxygen ratio and amount of total gas flow on the particle temperature and velocity. Furthermore, splats and coatings were deposited to investigate the relationship between diagnostic data, melting behavior and droplet substrate interactions. Such a comprehensive study, coupled with property measurements of the coatings, demonstrates critical operational variables among deposition procedure, coating microstructure and the deposit properties.

Introduction

Thermal sprayed ceramic coatings, such as alumina, zirconia and cordierite, offer a cost-effective alternative to modify the component surface properties and are widely applied as thermal barrier and wear resistance coatings. Typical wear resistance applications range from large pipes and paper machine rolls to smaller objects such as fiber guides and sleeves [1, 2]. Thermal sprayed ceramic coatings also show interesting electrical properties and can be considered to offer an economical solution as dielectric coatings in a variety of thick film and insulated metal substrate based electronics applications [3]. Extensive development work on plasma sprayed coatings has being carried out [2, 3], but recent studies have shown that HVOF is capable of depositing dense ceramic coatings [4–6]. The high velocity operational regime promotes an overall dense structure and. is considered an important benefit in numerous applications involving requirements for corrosion and wear as well as electrical insulation resistance. The HVOF process, being an enhanced combustion process, allows for acceptable deposition efficiencies of ceramic particles through axial injection of feedstock powders. However, due to the lower flame temperatures achievable when deposited by HVOF as compared to the plasma spray process; this form of thermal spray has yet to be successfully utilized for the production coatings [6]. Advanced characterization has revealed the difference in pore structure between air plasma sprayed (APS) and HVOF sprayed alumina coatings observed previously, showing the existence of lamellar/globular porosity for APS coatings compared to inter-pass layered porosity for HVOF coatings [7, 8]. This "sandwich structure" of the HVOF coating, where the porosity is concentrated on the inter-pass layer boundaries can

partly explain the difference in properties observed for HVOF sprayed alumina in comparison with APS sprayed alumina.

On-line diagnostic is an effective tool to comprehend issues between different spray parameters and particle behavior in the flame. Although a number of published studies exist for the plasma spray process diagnostics, there has been limited focus on the high velocity processes [9–12]. In these studies it has been shown that altering the gas flows and mixing ratios, i.e. the ratio of fuel to oxygen, will influence both the flame temperature and velocity, thereby influencing flame-particle interactions and coating development.

The studies presented in this paper focus on gaining a systematic understanding of the influence of processing conditions (fuel gas/oxygen ratio, total gas flow and particle flux) on microstructure development in HVOF alumina coatings. The effects of fuel gas/oxygen ratio on the melting level of the particle, total gas flow and particle flux in terms of coating thickness per pass on the properties of the coatings are presented in this paper. In-flight diagnostics, coupled with single splat studies, provide insights into particle behavior in the combustion zone and upon impact, thus allowing comprehension and establishment of salient processing-microstructure-property relationships.

In addition to process studies, experiments were carried out to deliberate to change the microstructure development process in order to examine the role of spray pass interfaces on various physical, thermal and electrical properties of the HVOF coatings. Past studies [7, 8] have shown that in HVOF process the high flattening ratio enables high density of deposits with low surface roughness, however, a new category of interfacial defects are observed in the interpass region as the torch travels in and out of the substrate. Studies have shown these interpass morphologies play a dominant role in through thickness thermal conductivity and interface fracture. In this study, attempts were made to produce such interpass interfaces of different density. Such integrated studies not only shed light into microstructure-property relationships but offer additional strategies for design and process optimization.

Experimental procedure

Spray test setup: Coating deposition and spray diagnostics were accomplished with a Praxair HV-2000 spray gun, fitted with 22 mm and 19 mm combustion chambers allowing for varying process parameters. Nitrogen was selected to be used as a carrier gas, and propylene (C_3H_6) and hydrogen (H_2) as fuel gases. A two-axis traverse unit with a rotating spindle was used to manipulate the gun and substrates during coating deposition. Feedstock powder was Praxair Al-1110HP, 99.3% Al_2O_3, with a nominal size of -22/+5 μm. Such a small particle size is required in the case of HVOF in order to provide sufficient heating of the material to ensure melting and efficient deposition.

Diagnostics: In-flight diagnostics were carried out at different spray conditions to measure the particle velocity, temperature and diameter using the Tecnar DPV-2000 system. Measurement distance was varied between 150 and 200 mm. The DPV-2000 uses infrared pyrometer along with a dual slit optical device to perform measurements on individual particles [13]. The instrument relies on the basic principle, where a hot particle passes through the measurement volume, emits energy into the sensor head in the form of a two-peak signal due to the double slit geometry of the photomask in front of the lens. Since the physical distance between the slits (~210 μm) as well as the time between signal peaks are known, the velocity of the particle can be determined. The particle temperature is measured using a dual color optical pyrometer, which references the temperature based on energy emission at two discrete wavelengths. The diameter of a particle is estimated by the time integral of the complete signal normalized for velocity. Additionally, the sensor head is mounted on an X–Y traverse unit, which permits mapping of the spray plume.

Splat test: Single splats were collected onto polished stainless steel plates by spraying a single pass with low powder feed rate. Splats collected were observed by optical microscopy, to determine the extent of melting of the alumina particles. While the temperature data from diagnostic tests, based on the emissivity of a particle in-flight, provides the surface temperature of the particle, single splats enhance our understanding on the particle state. In case of a material with high melting point and less residence time in the flame (owing to high velocity), such as alumina, the surface temperature will not reveal the melting of the core of the particles.

Coating preparation: Coatings were sprayed onto the steel plates with size of 25 mm × 50 mm × 2 mm for microstructural and property characterization and 50 mm × 100 mm × 2 mm for electrical breakdown studies. The microstructural development was controlled through traverse rate of the gun and rotational speed of the carousel, thus obtaining a certain thickness/pass. The aim of the spray tests was to generate coatings with the same total thickness by varying layer thickness per pass and amount of passes. The powder feed rate was between 10.5 g/min and 13.6 g/min. Spray distance was varied between 150 and 200 mm. The parameter combinations were similar for the splat and coating deposition.

Coating characterization: Microstructural characterization of the coatings was carried out under a Scanning Electron Microscope (SEM). The SEM used was a LEO 1550 model with a Schottky Field Emission gun, a standard Secondary Electron detector, an in lens Secondary Electron detector and a Back Scattered electron detector. Freestanding deposits were evaluated for porosity content using a Helium pycnometry technique. The skeletal density of the coating in this measurement is measured by volume of gas (Helium) displaced by a known mass of substance.

Thermal properties: Thermal conductivity measurements were carried out on a 12.5 mm (0.5") diameter disk, coated with carbon on both surfaces, using a Holometrix laser flash* thermal diffusivity instrument. In this test, the sample is irradiated uniformly on one side using a single laser beam pulse (1.06 μm wavelength). The temperature rise on the other side is recorded as a function of time using an HgCdTe infrared detector (2–5.5 μm wavelengths). The recorded temperature-rise data, with allowance for the measured sample thickness, are used to calculate the thermal diffusivity directly. Knowledge of the bulk density, together with the thermal diffusivity and specific heat, allows determination of the thermal conductivity [14].

Mechanical properties: Elastic modulus measurements were carried out on polished top-surfaces of the coatings bonded to the substrate. In this technique, depth-sensitive indentation method extracts the materials properties using the contact response of a small volume of material. In the present study, a spherical indenter was used. Continuous measurements of load/displacement curves were performed with a Nanotest 600 (Micro Materials Limited, Wrexham Technology Park, Wrexham, LL 137YP, UK) instrument using a 1.56 mm (1/16") WC-Co spherical indenter with a maximum load of 10N. The instrument enables a basic

load/displacement curve to be obtained, or multiple partial load/unload cycles to be performed. The load-displacement records were evaluated based on the Oliver and Pharr method [15] where the elastic modulus was determined from the elastic recovery part of the unloading curve.

Wear properties: The abrasive tests were performed using a rubber wheel and a quartz-sand abrasion tester according to ASTM G65. Samples were pressured against rubber wheel by using static normal force of 45 N. Sliding velocity was 1.2 m/s and sliding distance 2140 m. The abrasive sand for this test was rounded quartz particles with average size of 245 μm, and the sand mass flow was 270 g/min.

Electrical properties: Dielectric properties were measured using a HP 4294A Impedance Analyzer. Using parallel plate principles, the dielectric behavior was observed from 40 Hz to 100 MHz, the values at 10 kHz and 1 MHz are reported here.

Electrical strength of the coatings was tested according to IEC 60243-1 C1.9.1 by increasing the voltage up to the breakdown. Brass electrode, ∅25 mm, was used over the coating, and larger brass electrode, ∅75 mm, was placed under the specimen. The voltage was increased linearly from zero up to flashover by the rate of rise 0.03–0.05 kV/s.

Results

Diagnostics: Figure 1 and Figure 2 summarize findings of the diagnostic study from altering gas mixture, total gas flow and oxygen/fuel gas ratio. In Figure 3 is summarized the effect of different barrel lengths and stand off distances on the particle velocity-temperature behavior. The total gas throughput from the gun has a strong influence on the gas velocity and temperature for a given gas mixture ratio. For the experiments conducted, it was found that highest temperatures for propylene were obtained using a fuel gas/oxygen ratio of 0.30. In the case of hydrogen as fuel gas, highest temperature was obtained by using a ratio of 2.48 for the explored parametric space: Details of the influence of these parameter settings on the particle velocity and temperature are discussed later.

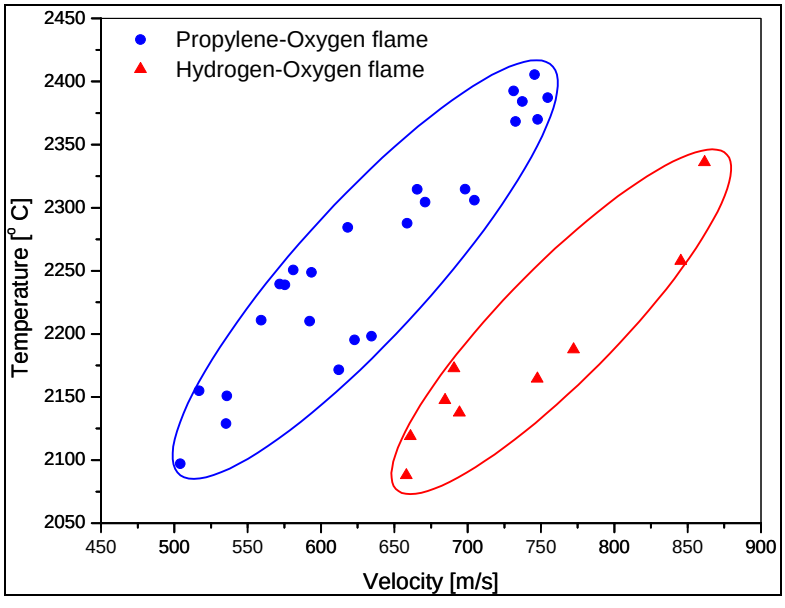

Figure 1. A first order process map for HVOF alumina depicting the range of particle temperatures and velocities for two fuel oxygen mixtures.

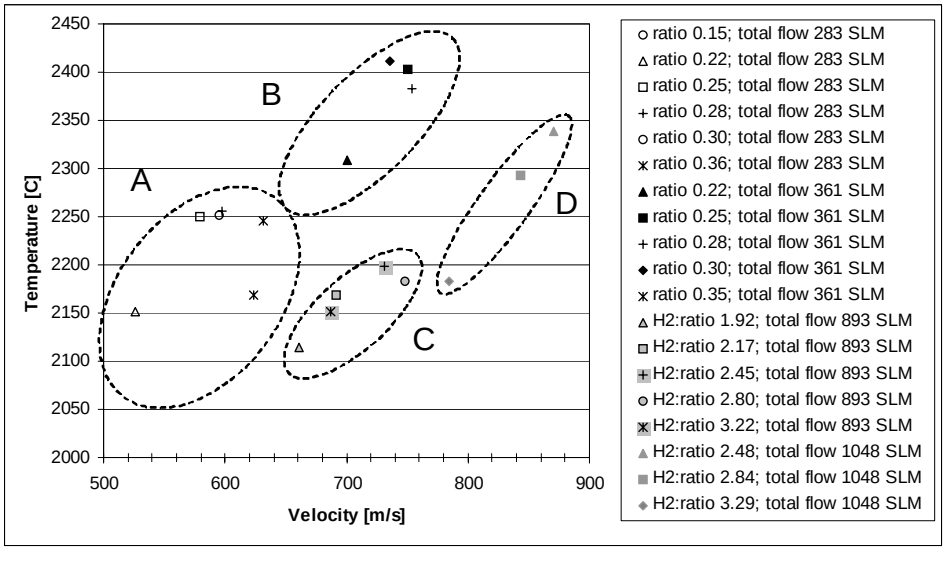

Figure 2. Process diagnostic data for different spray parameter combinations: Effect of total gas flow and gas flow ratio.

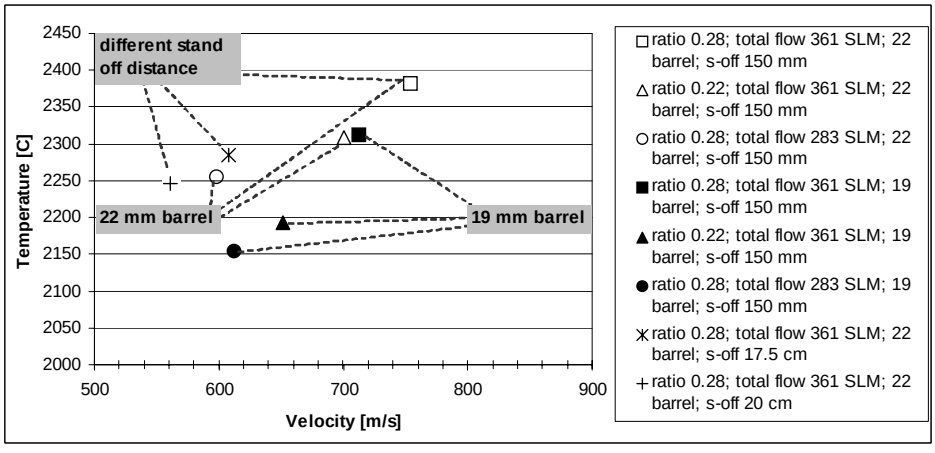

Figure 3. Process diagnostic data for different spray parameter combinations: Effect of barrel size and standoff distance.

Splat tests: Six spray parameter combinations were selected because of their influence on the single splats. The spray parameters used are listed in Table 1. Splats were produced to investigate the melting behavior of the particles. Wide range of splat morphologies observed is shown in Figure 4.

Table 1. Selected spray parameters and corresponding measured diagnostic data.

	Ratio C_3H_6/O_2	Total flow [l/min]	Stand off [mm]	T [°C]	v [m/s]
1	0.28	361	150	2390 ± 251	755 ± 120
2	0.22	361	150	2310 ± 204	700 ± 78
3	0.28	283	150	2210 ± 201	592 ± 86
4	0.28	361	200	2211 ± 159	560 ± 105
	Ratio H_2/O_2	Total flow [l/min]	Stand off [mm]	T [°C]	v [m/s]
5	2.48	1048	150	2339 ± 213	870 ± 124
6	2.17	893	150	2168 ± 170	692 ± 89

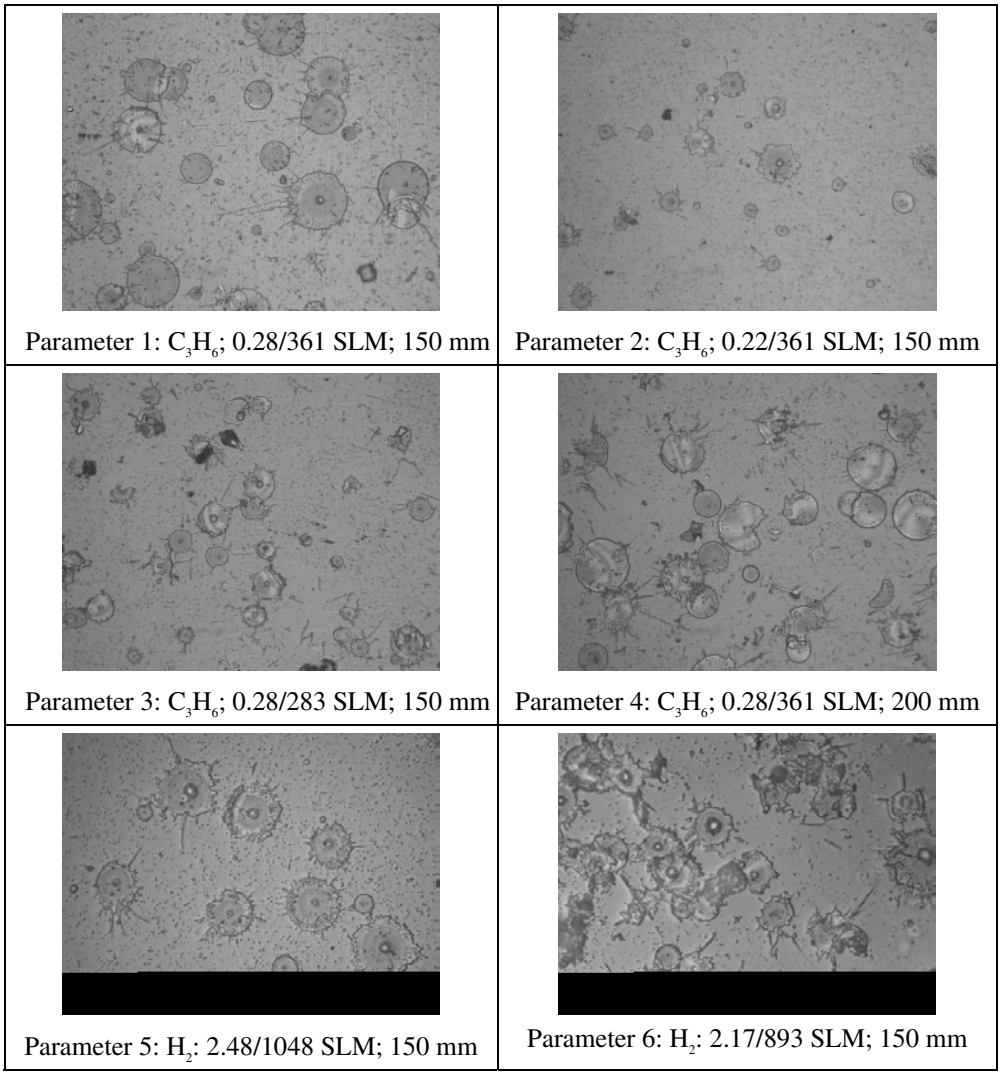

Figure 4. Micrographs depicting morphology of the splats collected at different spray parameters.

Deposition parameters: Coatings were sprayed with different fuel gas/oxygen ratios as listed in Table 2. All conditions from splat studies were selected. With condition 1 and 5, two variations of coatings were prepared varying thickness per layer. Total thickness was kept between 450–715 μm. Thickness per pass of the coating 'H' was found to be low due to poor deposition efficiency.

Table 2. Processing conditions for coating deposition.

	Ratio C_3H_6/O_2	Total flow [l/min]	Stand off [mm]	Thickness [µm]	Thickness/ pass [µm]
A	0.28	361	150	550	7.6
B	0.28	361	150	450	22.6
C	0.22	361	150	680	9.7
D	0.28	283	150	522	12.4
E	0.28	361	200	715	11.9
	Ratio H_2/O_2	**Total flow [l/min]**	**Stand off [mm]**	**Thickness [µm]**	**Thickness/ pass [µm]**
F	2.48	1048	150	620	4,8
G	2.48	1048	150	591	13,1
H	2.17	893	150	559	1,7

Coating characterization: A preliminary microstructural evaluation of the coatings was carried out using scanning electron microscopy (SEM). Microstructural details were examined looking at fractured surfaces, top surfaces and polished cross-sections. Figure 5 shows the top surface and fractured surface microstructures of coatings A, B and F. The top surfaces and the fractured surfaces of all the coatings look very similar. However, microcracking of the splats is observed on the top surface in each case in contrast to the single splat studies. A high magnification image is presented of the fractured surface showing well-adhered splats, indicative of complete melting (at least those that became part of the deposit). Figure 6 shows polished cross-section of the three coatings (A, B and F). The low magnification images show dense coatings with fine porosity while the corresponding high magnification images show detailed coating buildup. The formation of interpass porosity (corresponding to thickness per pass sprayed during processing) is observed for each of the three coatings.

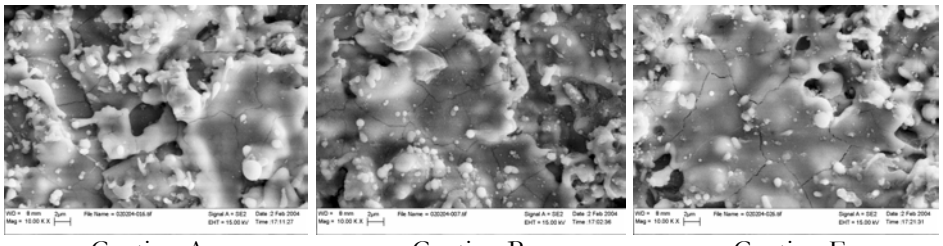

Coating A Coating B Coating F

Top surface

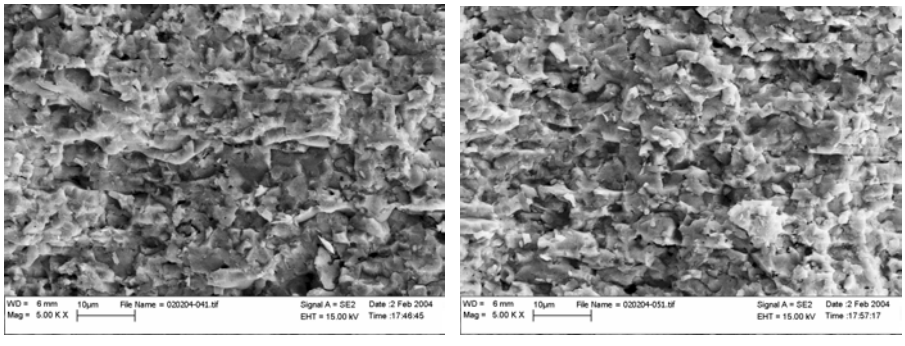

Coating A Coating F

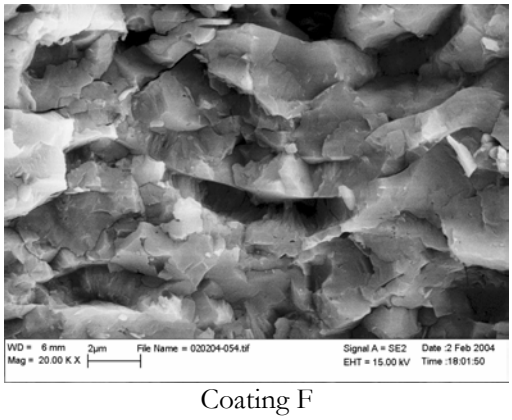

Coating F

Fractured cross-section

Figure 5. Top surface and fractured cross-section images of alumina coatings.

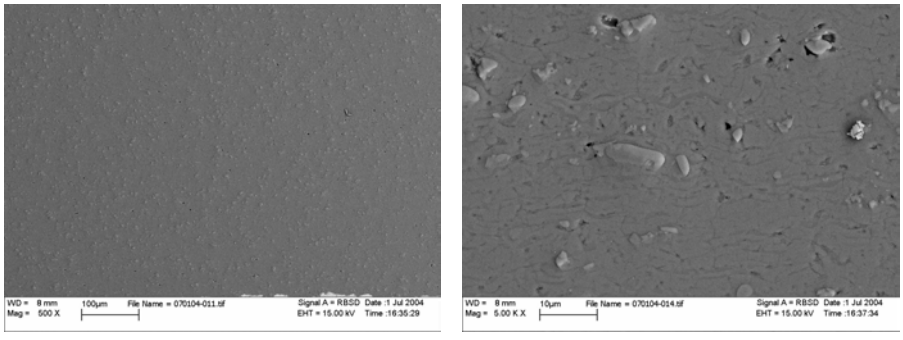

Coating A

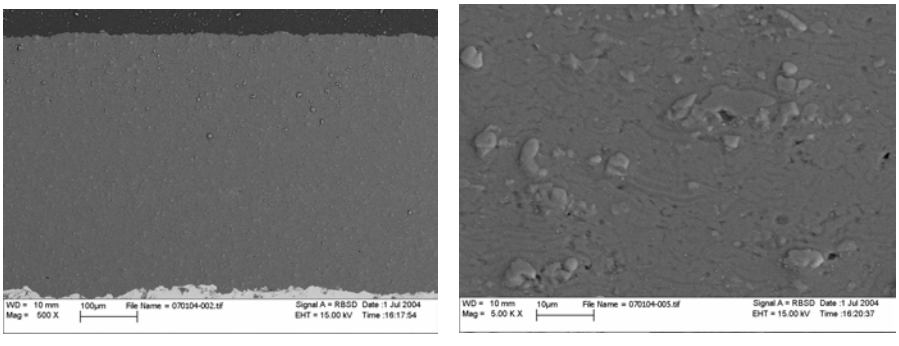

Coating B

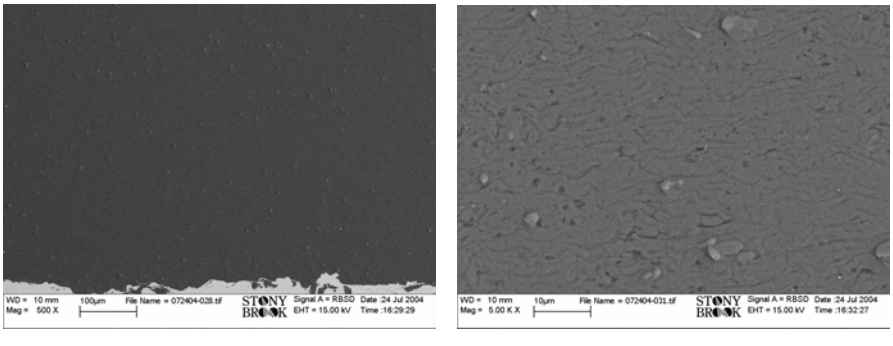

Coating F

Figure 6. Polished cross-section of alumina coatings, (A) low magnification images (500x) and (B) high magnification images (5000x).

Mechanical and thermal properties: Coatings were tested to compare the effect of different spray conditions and amount of interpass layering on the coating properties. In Table 3, density and elastic modulus for each coating is presented.

Not surprisingly, by using the hottest propylene and hydrogen parameters, highest density is obtained. As expected, density decreases as the melting status decreases.

Table 3. Density, Elastic Modulus and thermal conductivity of the coatings.

Sample	Density [g/cm³]	Elastic modulus [GPa]	Thermal conductivity [W/mK]
A	3.72	97 ± 6	3.88
B	3.70	100 ± 3	4.41
C	3.61	90 ± 4	3.74
D	3.65	99 ± 5	3.83
E	3.60	85 ± 2	3.58
F	3.72	100 ± 3	4.15
G	3.70	90 ± 5	3.86
H	3.66	97 ± 5	3.63

The variation in thermal conductivity for the eight coatings is also presented in Table 3. The overall thermal conductivity range was from 3.58 to 4.41. Similar to elastic modulus, thermal conductivity is lowest for the coating 'E' (sprayed at 200 mm standoff distance). Figure 7 (a) shows the thermal conductivity of the samples A–E plotted against number of interfaces normalized/mm for the coatings.

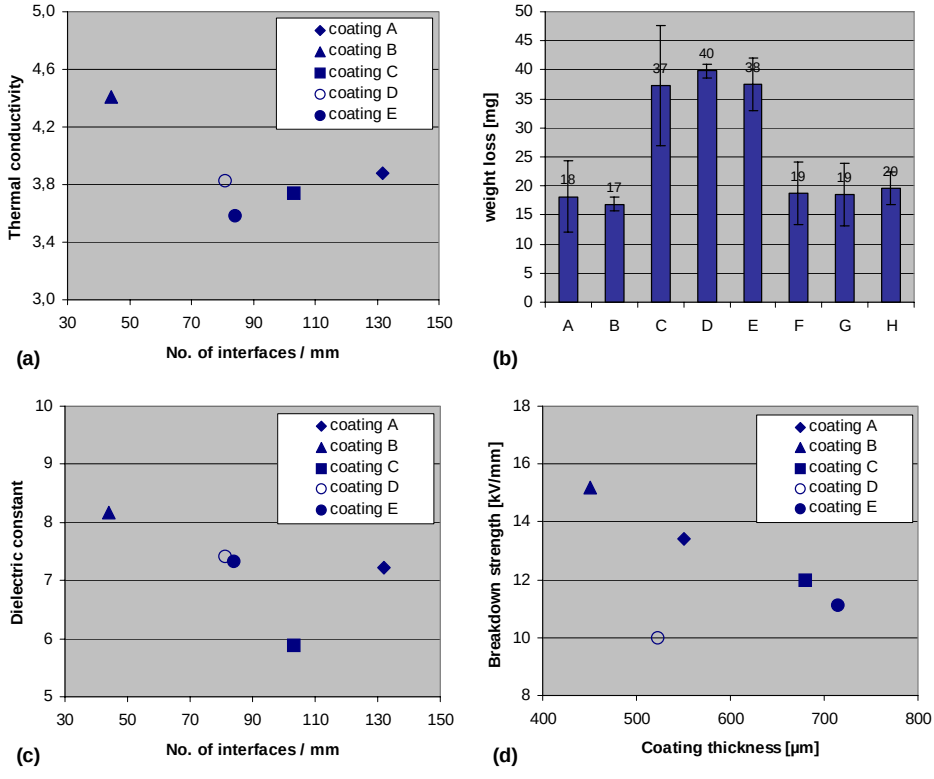

Figure 7. Mechanical, thermal and electrical properties of the coatings (a) Thermal conductivity, (b) Abrasive wear, (c) Dielectric constant, (d) Electrical breakdown strength as a function of coating thickness.

Electrical properties: The dielectric values were measured at 10 kHz and 1 MHz. Figure 7 (c) shows the dielectric behavior at 10 kHz for the samples A–E plotted against number of interfaces normalized/mm for the coatings. The dielectric constant varied from 5.9 to 8.2. An identical trend was observed when using 1 MHz. A clear correlation between number of interfaces and dielectric constant was again found. As the number of interpass interfaces increased, the dielectric constant was reduced.

The electrical breakdown studies were also performed for the coatings A–F. In the case of inhomogeneous thermal spray coatings, the breakdown always occurs at the "weak spot". It has been studied that mechanisms involved in the breakdown are mainly based on the corona discharge, which typically occur in the surrounding

medium such as voids and cracks. If electrical discharge and formation of the complete failure path is the main mechanism, the coating is damaged. Breakdown can partly operate in combination with thermal mechanism, in which case cumulative heating develops local paths with high electric field intensities. In this case, no definitive damage of the coating occurs [16].

Dielectric breakdown measured for the coatings sprayed by using propylene is presented versus thickness in Figure 7 (d). In all cases, electric arc occurred directly under the brass electrode. Upon repeated measurements at the same spot, only the main breakdown spot was left outside the electrode. Same values were obtained, which suggests that cracking and/or formation of major failure paths within coating under the test electrode does not occur. A small region (dia. 0.1–0.4 mm) was damaged within the main spot during breakdown.

Discussion

Diagnostics: The resulting 'Process map' for alumina in the temperature (T) – velocity (V) space is depicted in Figure 1. It must be noted that the operating range of the gas flows and fuel to oxygen ratios are quite different for the two mixtures. Two clear regions of different T and V arise from the use of different fuel gases. The hydrogen – oxygen mixtures typically resulted in greater velocity of the particles. Within each fuel gas, the effect of gas chemistry on the flame and resulting particle condition was examined by varying parameters such as fuel gas to oxygen ratios, total gas flow rates and different standoff distances. Conventional limits of gas ratios and flows were exceeded to obtain a wide velocity-temperature range.

A closer look at the effect of total gas flows and gas ratios is provided in Figure 2. It summarizes findings of the diagnostic study from altering total gas flow and oxygen/fuel gas ratio. In this figure, (A) and (B) refer to the zones of velocity and temperature achieved by using a gas mixture of propylene and oxygen while maintaining a total gas flow of 283 l/min and 361 l/min respectively. On the whole, there is a strong correlation between the velocity and temperature since the two total flow rate zones are separated quite clearly. A similar effect can be seen from (C) and (D) which are the values for hydrogen – oxygen gas mixtures with total flow rates of 893 l/min and 1048 l/min. Within each group of conditions, there is a

systematic variation of particle condition depending on the operating parameters. This variation is examined in detail in Figure 8.

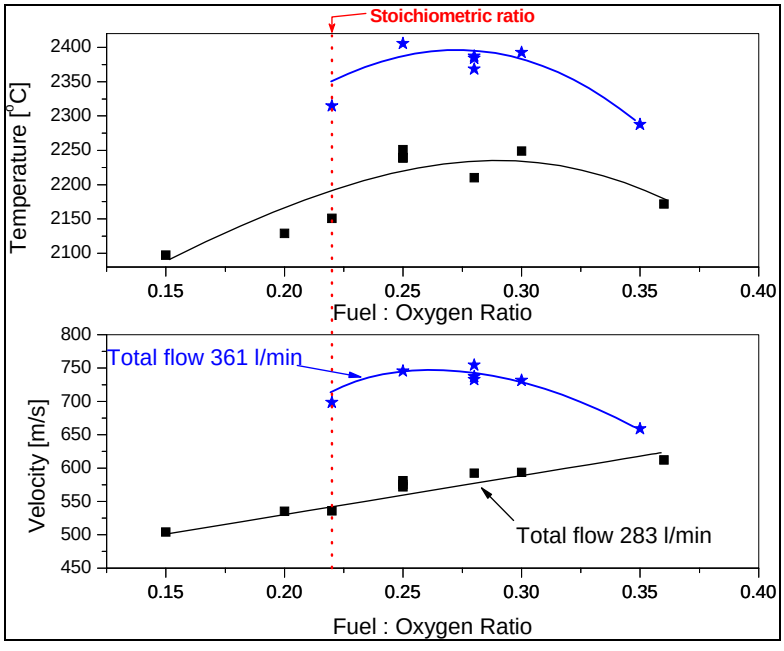

Figure 8. Variation in particle temperature and velocity as a function of fuel to oxygen ratio and total gas flow rates.

Figure 8 depicts the variation in particle temperature and velocity as a function of the fuel to oxygen ratio for two different total gas flow rates. Clearly, the total gas throughput through the gun has a strong influence on the gas velocity and temperature at a given ratio. The temperature increase in going from low to high flow rate seems to be uniform across all ratios. The change in particle velocity is not so uniform. In case of the high total flow rate condition, the velocity maximum coincides with the temperature maximum at a value of 0.30 i.e. the gas mixture had to be set to a fuel rich condition to achieve the maximum temperature for a fixed gas flow rate. For the lower flow rate conditions, the velocity values do not show a clear maximum. The values at stoichiometric ratio (0.22 as marked with the line) were found to be much lower than the maximum values recorded. The total gas flow could not be exceeded beyond 361 l/min due to safety and equipment considerations. It is expected that if the total gas flow was increased continuously, there would not be accompanying rise in temperature beyond an optimum point.

The velocity of particles is predominantly affected by the momentum of gases. Therefore, it would be more reasonable to evaluate temperature and velocity changes with respect to the total mass flow rate of the gases (since the nozzle opening is fixed, the increase in mass flow rate would correspond to an increase in the momentum of gases flowing through the torch). Such a comparison is provided in Figure 9. As can be seen, there is an almost linear increase in both velocity and temperature for a given ratio as the total mass flow rate of gases is increased (sample line drawn at common ratio value at all mass flows). Safety issues limited the range of mass flows that could be examined but it can be hypothesized that at sufficiently high mass flow rates, there will be a saturation or decrease in temperature due to incomplete combustion.

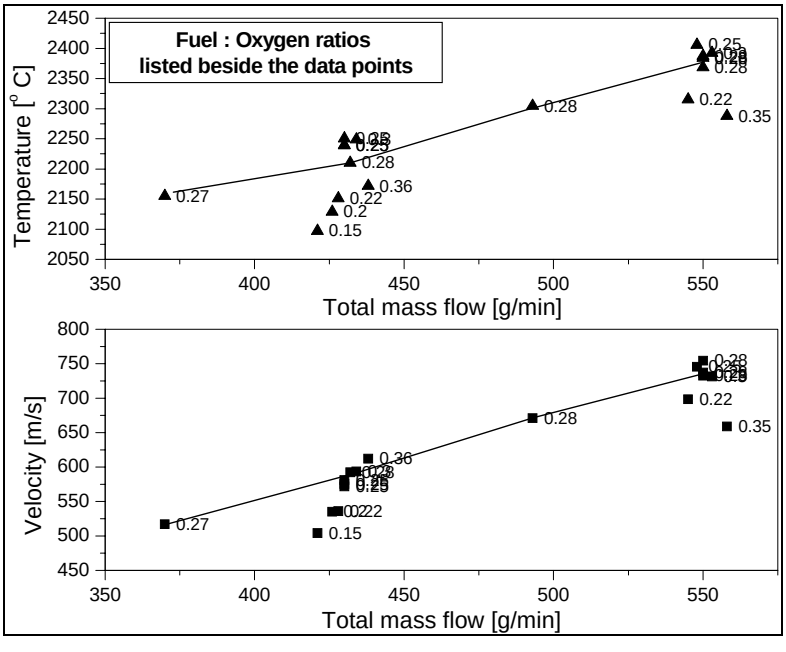

Figure 9. Velocity and temperature change as a function of total mass flow rate and ratio.

When using hydrogen, similar trends with lower temperatures but higher velocities were recorded. This is consistent with what has been reported before [12]. By increasing the amount of oxygen, particle temperature was seen to increase initially, but before the stoichiometric point, maximum value was obtained and subsequently there was a decrease in temperature.

Effect of using a longer and shorter combustion chamber (22 mm and 19 mm) and the effect of changing spray distance are shown in Figure 3. Comparing performance of combustion chambers, it is seen clearly that the length has a significant effect on the particle temperature but not on the velocity. A longer length of the nozzle seems to allow for better combustion of gases and heat transfer to the particles thereby raising the temperature, but velocity is governed more by the throughput of gases.

The effect of standoff distance on particle conditions was examined for three different spray distances. As seen in Figure 3, the highest velocity and temperature point is that measured at shortest spray distance (150 mm), the one with medium values at 175 mm and the lowest velocity and temperature point at 200 mm. Over the range of spray distances studied, temperature drop is not very significant (5%), but the change in velocity is (25%). The particles at longer distance have longer dwell times due to decrease in velocity as well as the longer spray distance. This results in better melting of the particles and is reflected in the splat formation as discussed below. It should be mentioned that with increasing spray distance, the divergence of spray plume also increases. This leads to a wider 'footprint' during coating and a change in thickness per pass of the deposit.

Splat tests: Different temperature-velocity points were selected to investigate of the particle surface temperature on the melting behavior of particle. It is evident that the particle wetting and flattening is dependent on the particle conditions in the flame. The best wetting was obtained for the parameter 1 producing highest Tp, Vp with maximum melting behavior. By decreasing particle temperatures and velocities, the largest particles were insufficiently melted and bounce away from the substrate (parameter 2).

Effect of particle flight time in the flame was demonstrated with parameters 3 and 4. With these two parameters, the data obtained from diagnostic measurements were identical but at different stand off distances. However, as discussed earlier particles melting efficiency was higher for those at extended stand off distance (parameter 4). This is evident from Figure 3 where the splat shape and splat density difference is seen. Splats set condition 5 and 6 were sprayed by using hydrogen as a fuel gas with two different total gas flows and ratios. Diagnostic studies showed that parameter set 5 gives slightly lower maximum particle temperatures, but higher velocities. Condition 6 was selected for comparison of lower and higher particle

temperature and velocity to the melting stage of the particle. Melting is good with both hydrogen parameters. In general the H2 condition resulted in a larger degree of fragmentation compared to the propylene conditions (comparing parameters 1 and 4). This is attributed to increased particle velocities.

Coating characterization: The intrinsic properties of the individual splats and their buildup in formation of the coating are affected by the in-flight feedstock-particle properties within the flame (i.e., their temperature, velocity, size, and degree of melting). From the high magnification images (Figure 6) the distinct features, corresponding to thickness per pass sprayed during processing, are observed in all three coatings. The coatings were deposited with different conditions (A with 7.6 μm per pass, B with 22.6 μm per pass and F with 4.8 μm per pass). This is evident in the high magnification images where maximum numbers of interfaces are observed for the coatings F and A as compared to coating B. This will influence coating properties as discussed below.

Mechanical properties: Decrease in density of the thermal sprayed coatings compared to the bulk density is a combination of the interlamellar pores, globular pores and cracks. However, the HVOF coating shows well-adhered splats with finer porosity compared to the plasma sprayed coatings [8]. The lower surface roughness for the top surface of the HVOF coating (compared to plasma spray) results from the use of a finer powder, from enhanced splat flattening, and from the smooth surface of the individual splats collected [3].

Clear correlation between diagnostic studies and melting stages of the particles obtained from the single splats can be observed. Highest density values are obtained with the hottest propylene and hydrogen parameters. Elastic modulus measured for the coatings correlates well with this observation, having highest modulus for the coatings having highest density. However, overall no strong differences in elastic modulus were observed. The low modulus of coating 'C' can be attributed to the low fuel/oxygen ratio compared to others. The coating 'E' showed the lowest modulus of all since it is sprayed at 200 mm standoff distance, compared to 150 mm for all others. This again correlates well with the lower particle velocity at increased standoff distances.

Wear resistance of the coatings also correlates with the particle state, and especially with the melting stage of the particles. Coatings deposited using hottest parameters,

had the best abrasive wear resistance. In the case of hydrogen, the effect of the total gas flow rate or the gas ratio is not that strong as compared to the coatings manufactured by using propylene.

A clear correlation between number of interfaces and dielectric constant was found. The behavior was similar to the thermal conductivity. In the case of high deposition rate (Coating 'B' with 22.6 μm per pass) there exist very few interfaces, thus giving highest thermal conductivity among all coatings. Coating A is sprayed with exactly same condition, but the thickness per layer is 7.6 μm per pass decreasing thermal conductivity of the coating. For all other coatings, there exist increasing amount of porosity between layers due to interpass layering effect, thus lowering the thermal conductivity. Spray parameters and flattening rate of the splats also effect the thermal conductivity. For coating 'E' having highest porosity due to the longer standoff distance the lowest thermal conductivity is measured.

Lower deposition rate leads to larger number of interpass interfaces, resulting in a lower dielectric constant. The interpass region can be treated as air gap resulting in a composite capacitor with alumina and air. Modeling work is underway to develop a constitutive relationship between this composite microstructure and dielectric properties.

The breakdown strength strongly depends on the coating thickness and follows the same trend as those reported in the literature for thermal spray coatings [3]. Breakdown voltages measured are presented in the Figure 7 (d) and are as follows for the various samples: a) 7.3 kV, b) 6.7 kV, c) 8.2 kV, d) 5.3 kV, e) 8.0 kV, f) 9.6, g) 9.4, and h) 9.4. It can be assumed that formation of the critical failure path is not linearly dependent on the coating thickness. After certain threshold value is exceeded, formation of the critical failure path is faster. Partly this is introduced by increased vertical cracking when coating thickness is increased. However, when results are normalized with coating thickness, better values are obtained for the thinner coatings.

These studies have shown that a combination of particle parameters and deposit build-up strategies can be used to manipulate and control coating properties. Establishing process-particle state correlations concurrently with microstructure-property relationships will ultimately enable new design strategies for coatings.

Conclusions

An integrated study with respect to processing, microstructure and properties of HVOF alumina was undertaken to understand each aspect of this chain. A spectrum of temperature velocity regimes can be obtained by varying process parameters such as fuel gas mixtures, fuel gas/oxygen ratio and total gas flow resulting in a range of melting states for the particles along with different kinetic energies. It is observed that a wider melting spectrum is demonstrated by the propylene – oxygen system. This can have implications for both – a larger control domain for the particles (and thus coating properties) if the process is controlled, or a wider variability in properties if the process control is inadequate.

It has been shown that the particle temperature and the melting state control the deposit efficiency and the build-up rate while the flattening behavior is dominated by particle kinetic energy.

The coating density and mechnical properties are strongly affected by particle velocity when complete melting is achieved. The particle state in the case of HVOF is very sensitive to the standoff distance and is found to be an influential parameter controlling microstructure and properties.

It has been noted that in HVOF the inter-pass interfaces play a dominant role in thermal, electrical and tribological properties. This is attributed to the large flattening degree of HVOF splats compared to their plasma spray counterparts. This introduces an additional degree of freedom with respect to property control. By varying coating build-up rate (through a combination of feedrate and robotic trajectory management), different interpass porosity structures were created in the coating. Clear correlations were obtained between nature of pore architecture with the thermal and dielectric behavior.

Such systematic and integrated studies enable a science based approach to coating development and optimization and ultimately provide a foundation for coating integrated component design.

Acknowledgement

This work was sponsored by the MRSEC program of the National Science Foundation under award DMR – 0080021 and by TEKES, National Technology Agency of Finland.

References

[1] Damani, R.J. & Makroczy, P. Heat treatment induced phase and microstructural development in bulk plasma sprayed alumina. Journal of the European Ceramic Society 20(2000), pp. 867–888.

[2] Ramachandran, K., Selvarajan, V., Ananthapadmanabhan, P.V. & Sreekumar, K.P. Microstructure, adhesion, microhardness, abrasive wear resistance and electrical resistivity of the plasma sprayed alumina and alumina-titania coatings. Thin Solid Films, 315(1998), pp. 144–152.

[3] Swindeman, C.J., Seals, R.D., Murray, W.P., Cooper, M.H. & White, R.L. Proceedings of the 9th National Thermal Spray Conference; Practical Solutions for Engineering Problems, ASM, Cincinnati, OH, USA, October 7–11, 1996, pp. 793–797.

[4] Thorpe, M.L. & Richter, H.J. A Pragmatic Analysis and Comparison of HVOF Processes. J. Therm. Spray Technol. 1, 2(1992), pp. 161–170.

[5] Sturgeon, A.J., Harvey, M.D.F., Blunt, F.J. & Dunkerton, S.B. Proceedings of 14th International Thermal Spray Conference. Current status and future trends, High Temperature Society of Japan, Kobe, Japan, May 22–26, 1995, pp. 669–673.

[6] Dent, A.H., Patel, A., Gutleber, J., Tormey, E., Sampath, S. & Herman, H. High velocity oxy-fuel and plasma deposition of BaTiO3 and (Ba,Sr)TiO3. Materials Science and Engineering B87(2001), pp. 23–30.

[7] Kulkarni, A., Sampath, S., Goland, A., Herman, H. & Dowd, B. Computed microtography studies to characterize microstructure-property correlations in thermal sprayed alumina deposits. Scripta mater. 43(2000), pp. 471–476.

[8] Kulkarni, A., Gutleber, J., Sampath, S., Goland, A., Lindquist, W.B., Herman, H., Allen, A.J. & Dowd, B. Studies of the microstructure and properties of dense ceramic coatings produced by high-velocity oxygen-fuel combustion spraying. Materials Science and Engineering A369(2004), pp. 124–137.

[9] Ignatiev, M., Smurov, I. & Bertrand, P. Proceedings of International Thermal Spray Conference. (ITSC 2002), DVS, Essen, Germany, March 4–6, 2002, pp. 72–77.

[10] Hearley, J.A., Little, J.A. & Sturgeon, A. J. The effect of spray parameters on the properties of high velocity oxy-fuel NiAl intermetallic coatings. Surface and Coatings Technology 123(2000), pp. 210–218.

[11] Arsenault, B., Legoux, J.G., Hawthorne, H., Immarigeon, J.P., Gougeon, P. & Moreau, C. HVOF process optimization for the erosion resistance of WC-12Co and WC-10Co-4Cr coatings. International Thermal Spray Conference 2001, Singapore; 28–30 May 2001, pp. 1051–1060.

[12] Lugscheider, E., Herbst, C. & Zhao, L. Parameter studies on high-velocity oxy-fuel spraying of MCrAlY coatings. Surface and Coatings Technology 108–109(1998), pp. 16–23.

[13] Blain, J., Nadeau, F., Pouliot, L., Moreau, C., Gougeon, P. & Leblanc, L. An Integrated Infrared Sensor System for On-Line Monitoring of Thermally Sprayed Particles. Proceedings, 10th International Conference on Surface Modification Technologies, SMT-10, Singapore, 2–4 Sept. 1996, pp. 677–686.

[14] Parker, W.J., Jenkins, R.J., Butler, C.P. & Abbott, G.L. Flash Method of Determining Thermal Diffusivity, Heat Capacity and Thermal Conductivity. J. Appl. Phys. 32, 9(1961), p. 1679.

[15] Oliver, W.C. & Pharr, G.M. An Improved Technique for Determining Hardness and Elastic Modulus Using Load and Displacement Sensing Indentation Experiments. J. Mater. Res. 7(1992), pp. 1564–1583.

[16] Kim, H.-J., Odoul, S., Lee, C.-H. & Kweon, Y.-G. The electrical insulation behaviour and sealing effects of plasma sprayed alumina-titania coatings. Surface and Coatings Technology 140(2001), pp. 293–301.